# Experimental investigation of the pressure drop in porous ceramic diesel particulate filters

**G A Stratakis, D L Psarianos** and **A M Stamatelos***
Mechanical and Industrial Engineering Department, University of Thessaly, Volos, Greece

**Abstract:** Understanding of the mechanisms that affect flow and pressure drop in porous ceramic diesel particulate filters is important in the design optimization of this class of diesel exhaust after-treatment systems. Furthermore, determination of the parameters involved in the calculation of pressure drop as a function of collected soot mass is important for successful filter loading and regeneration modelling. This paper presents the results of an experimental analysis of pressure drop as a function of the geometric and operating parameters of cordierite and SiC diesel filters. Single-cell filters from cordierite and silicon carbide were prepared to single out any effects from the complex flow processes that take place in a full-sized filter. The product of soot layer permeability and density was experimentally determined by employing a specially designed experimental apparatus. The calculation was supported by a simple computer calculation that is also presented in this paper. The distribution of soot loading inside the channels of a full-sized filter, in various loaded and partially regenerated conditions, was assessed by connecting the apparatus to discharge through selected channels of the filter. The results are shown to improve understanding of the effects of partial regeneration and fuel additive residuals on filter back pressure and flow and soot loading distribution.

**Keywords:** diesel particulate filters, pressure drop, flow maldistribution, diesel soot permeability, regeneration, fuel additives

## NOTATION

| | |
|---|---|
| $A$ | area ($m^2$) |
| $C_D$ | discharge coefficient |
| $dm_i$ | mass discharged at the $i$th time step (kg/s) |
| $E$ | substrate thickness (m) |
| $k$ | permeability ($m^2$) |
| $L$ | single-channel filter length (m) |
| $m$ | mass (kg) |
| $m_v$ | mass of air present in the vessel (kg) |
| $\dot{m}_{real}$ | real mass flowrate (kg/s) |
| $Ma$ | Mach number |
| $p_T$ | throat pressure (Pa) |
| $p_{Tc}$ | calculated pressure in the throat (Pa) |
| $p_{TG}$ | guessed pressure in the throat (Pa) |
| $p_0$ | vessel (identical to stagnation) pressure (Pa) |
| $R$ | ideal gas constant [$R_{air} = 287$ kJ/(kg K)] |
| $t$ | time (s) |
| $T$ | temperature (K) |
| $T_0$ | stagnation temperature (K) |
| $u$ | velocity (m/s) |
| $U$ | mean filtration velocity (m/s) |
| $V$ | vessel volume ($m^3$) |
| $w$ | single-channel filter width (m) |
| $\gamma$ | specific heat ratio $c_p/c_v$ |
| $\Delta P$ | pressure drop across a single-channel filter (Pa) |
| $(\Delta P)_c$ | calculated pressure drop across a single channel (Pa) |
| $\mu$ | dynamic viscosity (Pa s) |
| $\rho$ | density ($kg/m^3$) |
| $(\rho k)_p$ | soot layer density times permeability product (kg/m) |

### Subscripts

| | |
|---|---|
| atm | atmospheric |
| c | calculated |
| ch | channel |
| f | filter |
| G | guessed |
| $i$ | time step |
| p | particulate |

*The MS was received on 23 January 2002 and was accepted after revision for publication on 20 June 2002.*
** Corresponding author: Laboratory of Thermodynamics and Thermal Engines, Mechanical and Industrial Engineering Department, University of Thessaly, Pedion Areos, GR-383 34, Volos, Greece.*

| | |
|---|---|
| real | not ideal |
| s | ceramic |
| T | throat |
| v | vessel |
| 0 | stagnation |

## 1 INTRODUCTION

The interest in diesel aftertreatment systems by the automotive manufacturers is ever growing, in view of increasingly stringent legislated emission standards [**1**]. As regards particulate emissions, the wall-flow particulate filter is today the most efficient aftertreatment device [**2**], attaining filtration efficiencies of over 90 per cent. Typical diesel particulate consists mainly of a carbonaceous core (soot formed during combustion), with adsorbed compounds such as unburned and partially oxygenated hydrocarbons (VOF), as well as sulphates and metal oxides [**3**]. The demand periodically to clean the filter by burning off (oxidizing) the collected particulate (filter regeneration) under unfavourable conditions of low exhaust temperatures met in modern diesel engine exhaust systems led to the wide application of catalysts [**4**–**7**]. The doping of the diesel fuel with catalytic additives (usually in the form of organometallic compounds) is today a workable catalytic regeneration technique. However, further design optimization of fuel additive assisted trap systems seems to be necessary to solve problems related to filter durability and additive ash accumulation. The support by an active regeneration strategy employing measures by the engine control unit (ECU) is usually employed in practice to secure the onset of regeneration above a specific soot loading threshold. Filter soot loading can only be indirectly assessed by the ECU, based on the recording of pressure drop, engine speed, exhaust temperature and fuel flowrate [**8**]. The above parameters, which the ECU needs to sense in order to assess the necessity of activating regeneration, are presented in Fig. 1. The estimation of soot mass as a function of pressure drop and engine operating parameters has proven to be a complex task. Furthermore, this dependence seems to affected by filter regeneration history, owing to the effects of soot remaining from previous, incomplete regeneration events. Such incomplete regeneration may be observed at the filter periphery because of the lower temperatures prevailing there. The effect of residual soot mass from a previous incomplete regeneration becomes prominent if filter loading curves of a new filter and a loaded and subsequently incompletely regenerated filter are compared, as in Fig. 2. In the two cases, the initial back pressure is approximately equal. However, the back pressure increase with loading at the same engine operation point (same particulate emissions) is observed to be much steeper with the partially regenerated filter.

On the other hand, design optimization of diesel par-

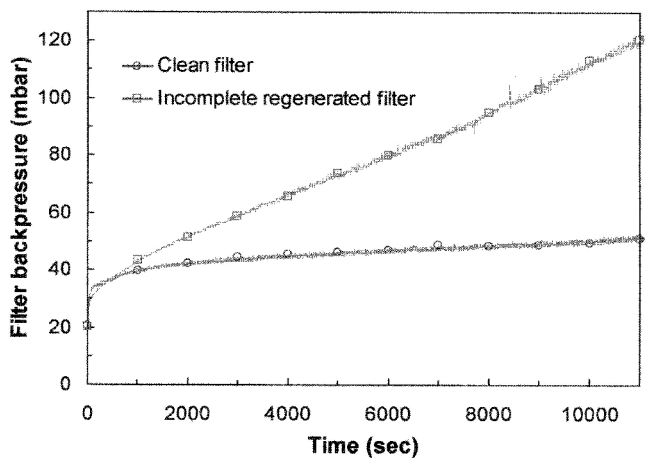


**Fig. 2** Loading curves for a clean and an incompletely regenerated filter (filter type SiC 14/200 143.8 × 152.4 mm, engine DW10ATED, speed 1250 r/min, torque 30 N m)

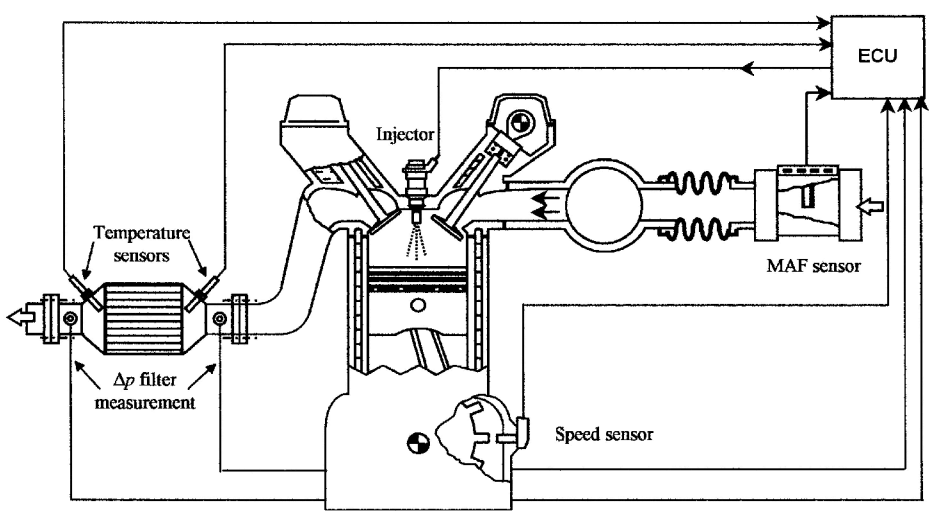


**Fig. 1** Schematic diagram of an active diesel particulate filter control system

 

ticulate filter systems is increasingly dependent on efficient modelling of the filter regeneration process [**9**]. A significant number of one-dimensional and even three-dimensional models have been presented in the literature [**10**–**13**], covering thermal and catalytic regeneration. The currently employed models should be able to predict the propagation of regeneration in the trap in the vehicle or engine bench installation by taking into account the dominating processes in the filter, namely [**14**]:

(a) filter back pressure as a function of geometric and operating parameters for different particulate loadings;
(b) thermal and chemical processes inside the filter, including heat transfer and particulate oxidation by exhaust oxygen (with or without the use of catalytic aids).

The main difficulty encountered in the validation of diesel filter regeneration models lies in the extraction of realistic particulate properties by the experiments. Tests with a real filter loaded and regenerated are more realistic than those with mini-scale filters and synthetic soot accumulation, but the operating conditions (particulate loading, flow distribution in the filter, exhaust gas properties) are more difficult to control. Better understanding of these effects are sought in this paper, by means of experimentally studying pressure drop and flow distribution inside mini-sized and full-sized filter specimens. A novel technique is developed that makes it possible to estimate with sufficient accuracy the product of soot layer permeability and soot density in a single filter channel. This is done by recording the discharge process of a vessel containing air, connected to the filter channel, that may be loaded with real exhaust gas at different engine operation points and up to different particulate loading levels. The vessel discharges through a specially designed nozzle, modified to be able to connect it directly to the channels of real filters of various cell sizes. Based on the processing of the experimental results, understanding of the soot mass and ash residual distribution between the different channels may be improved. Furthermore, incompletely regenerated regions of the filter can be spotted and understanding of the filter pressure drop can be improved.

## 2 FILTER PRESSURE DROP APPROXIMATIONS

The total pressure drop across the particulate filter wall can be expressed as the sum of the porous ceramic substrate pressure drop and the soot layer pressure drop [**14**]:

$$\Delta p = \Delta p_s + \Delta p_p \tag{1}$$

It is generally accepted [**14**, **15**] that the pressure drop associated with flow through ceramic filters can be approximated by Darcy's law. According to this law, the total pressure drop due to flow through the ceramic wall and the soot layer can be approximated by the following simplified relation:

$$\Delta p = \frac{\mu U E_s}{k_s} + \frac{\mu U E_p}{k_p} \tag{2}$$

By using the concept of effective particulate layer thickness [**14**], the latter formula can be rewritten as follows:

$$\Delta p = \frac{\mu U E_s}{k_s} + \frac{\mu U m_p}{A_f (\rho k)_p} \tag{3}$$

This formula allows, in principle, the backward approximate calculation of collected soot mass as a function of measured filter back pressure at a certain engine and filter loading operation point, once an approximate value for the product $(\rho k_p)$, that is, soot layer density times soot layer permeability, is known for the specific engine–filter–operation point combination.

Now, both factors of the above product are variable, and so the product $\rho k_p$ is widely varying, depending on engine type, injection pressure, filter type, operation point, possible use of fuel additives, etc. The wide dispersion (several orders of magnitude) of this product has already been mentioned by various researchers [**14**]. The aim of this paper is further to investigate these discrepancies and possibly narrow their range of variation by the previously mentioned experimental set-up, which is presented below in more detail.

## 3 EXPERIMENTAL

### 3.1 Single-channel filter specimens

In order to exclude any three-dimensional effects in the measurements, single-channel filters were prepared by breaking up two of the most frequently used filter types:

(a) a cordierite filter (17 × 100),
(b) a silicon carbide filter (14/200).

The properties of the two types of filter material are presented in Table 1. These single-channel filters are designed to be assembled to the engine exhaust pipe, as presented in Fig. 3. In the specific experiments presented

**Table 1** Properties of single-channel filters used for the experimental study

| Property | Cordierite | SiC |
|---|---|---|
| Material density (kg/m$^3$) | 2510 | 3080 |
| Porosity (%) | 43 | 42 |
| Cell size (mm) | 2.54 × 2.54 | 1.49 × 1.49 |
| Wall thickness (mm) | 0.6 | 0.4 |
| Wall density (kg/m$^3$) | 1000 | 1800 |
| Mean pore size (μm) | 33 | 9 |
| Permeability (m$^2$) | $0.64 \times 10^{-12}$ | $3.7 \times 10^{-13}$ |

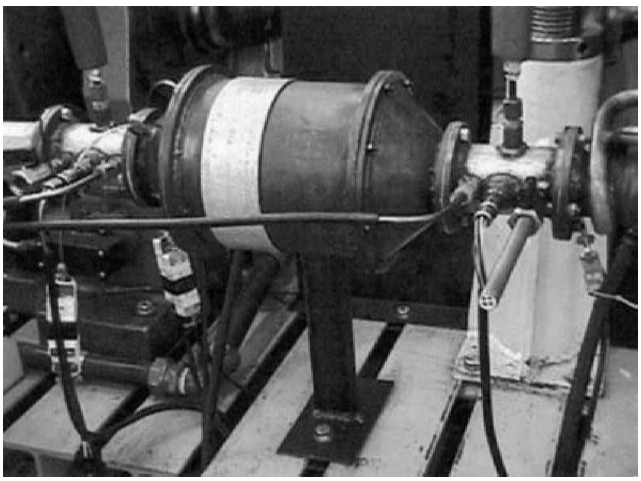

**Fig. 3** Mini-scale filter assembly on an engine exhaust system

in this paper, the minifilters were mounted in parallel to the full-sized diesel filter into the exhaust system of a 2.0 l HDI turbocharged passenger car engine, running on the LTTE engine test bed, with the engine specification given in Table 2. Figure 4 presents the experimental layout of the filter loading experiment. The full-sized filter employed in these experiments is an SiC 14/200 filter with the characteristics shown in Table 3.

### 3.2 Air expansion through the filter channel

Each single-channel filter, after being loaded with soot, may be connected to a vessel containing air at 1 bar initial gauge pressure. The vessel discharge pipe is controlled by a solenoid valve and opens on demand by the data acquisition software, triggering the expansion of the compressed air from the vessel through the channel walls to the atmosphere. Monitoring of the expansion process is carried out by means of recording the signal of a pressure sensor that is also mounted to the vessel. The layout of the measuring device is shown in more detail in Figs 5 and 6a.

**Table 2** Diesel engine specifications

| | |
|---|---|
| Manufacturer | PSA |
| Engine type | HDI turbocharged engine (DW10ATED) |
| Cylinders | 4, in-line |
| Displacement | 1997 $cm^3$ |
| Rated power/rated speed | 80 kW/4000 r/min |
| Maximum torque/speed | 250 N m/2000 r/min |
| Average fuel consumption | 5.5 l/100 km |

**Table 3** Diesel particulate filter specifications

| | |
|---|---|
| Manufacturer | Ibiden |
| Type | SiC 14/200 |
| Diameter | 143.8 mm |
| Length | 152.4 mm |
| Cell concentration | 200 cells/$in^2$ |
| Cell pitch | 1.89 mm |
| Wall thickness | 0.4 mm |

### 3.3 Experiments with a full-sized filter

In order indirectly to evaluate the soot loading distribution from filter centre to periphery, the design of the

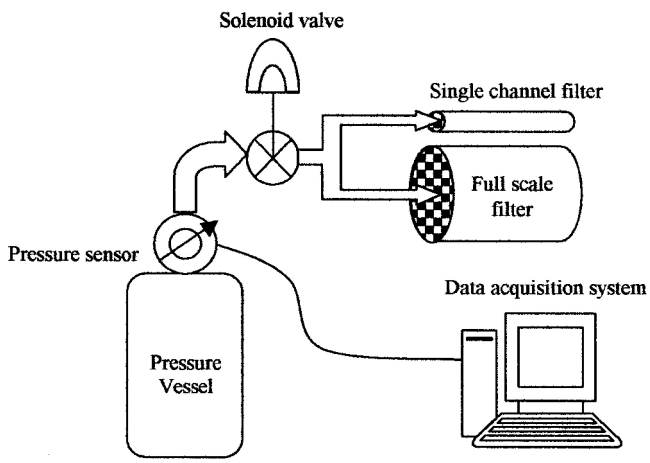


**Fig. 5** Schematic diagram of the measuring device

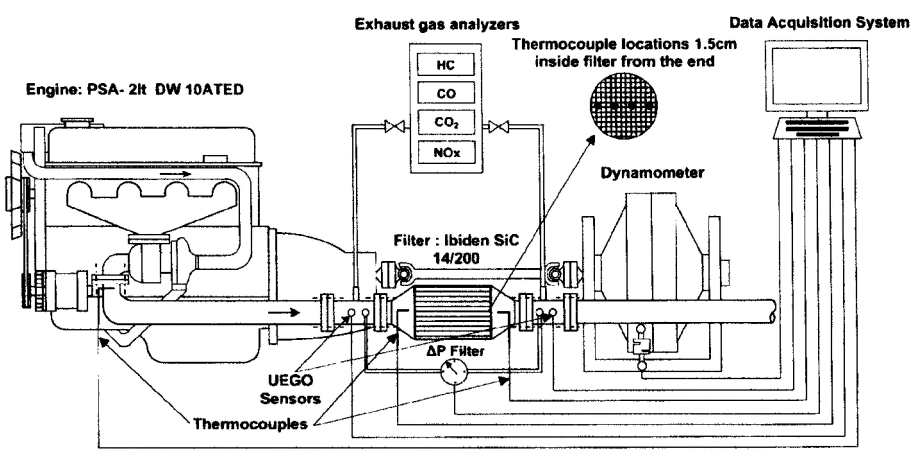


**Fig. 4** Experimental layout

 

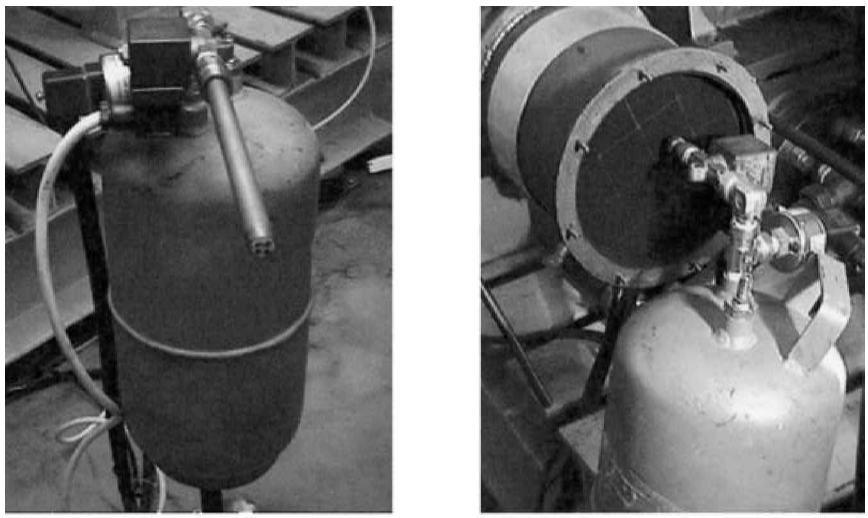


**Fig. 6** Use of the measuring device for (a) single-channel filter loading measurement and (b) full-scale filter channel loading distribution measurement

above device was improved in such a way that its nozzle was able to be tightly connected to selected inlet channels of the full-scale engine filter. The exhaust pipe of the vessel was carefully connected to the inlet of various trap channels, and the pressure drop characteristic was recorded as shown in Fig. 6b.

### 3.4 Measurement protocol

The following strategy is applied in the determination of the exact protocol for filter loading tests. Temperature and mass flowrate under full load and part load engine operating conditions, being more representative of city driving conditions, are mapped in Figs 7 and 8. The final design of the test protocol, based on the results of engine mapping, is presented in Table 4. The test protocol contains operation points lying at the lower left part of the engine map (low-to-medium speed by low-to-medium load) and, at each operation point, both single-channel and full-sized filters are loaded in parallel. Soot loading mass cannot be fixed in advance owing to the lack of knowledge of the function of mass versus $\Delta p$. After the completion of an approximate loading (order of 100 mbar independent of engine operation point), the expansion device can be fitted to both types of filter in order to perform measurements to assess soot loading. Especially for the case of the full-sized filter, the device is fitted to a number of characteristic channel inlets (Fig. 6b). After the end of the recording of the single-channel filter expansion process, the single-channel filter is weighed in order to obtain the amount of accumulated soot mass. Afterwards the filter is regenerated in order

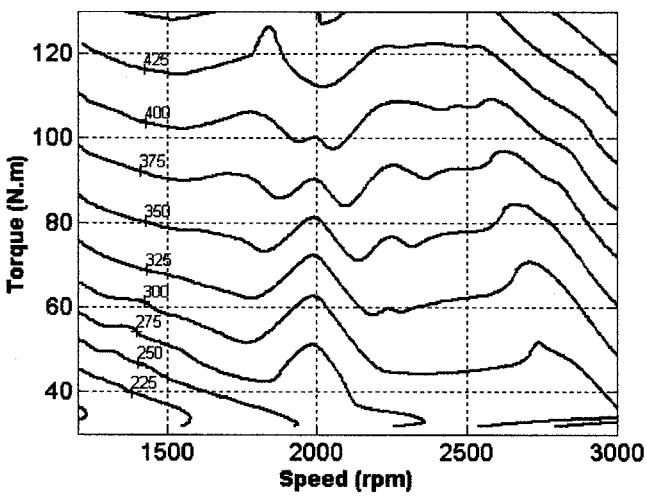


**Fig. 7** Map of the filter wall temperature (°C) at the centre-line, 15 mm from the filter exit

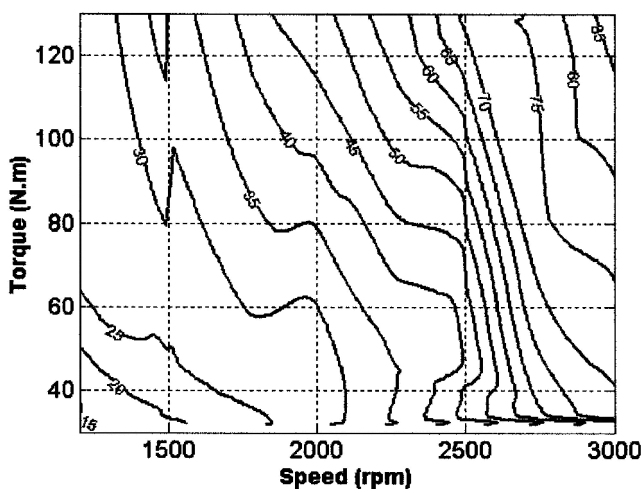


**Fig. 8** Map of the engine exhaust gas mass flowrate (g/s)

**Table 4** Experimental protocol

| Speed (r/min) | Torque (N m) | Mass flowrate (g/s) | Temperature of exhaust (°C) | Temperature of filter, inlet (°C) | Temperature of filter wall, centre (°C) | Temperature of filter wall, side (°C) |
|---|---|---|---|---|---|---|
| 1250 | 30 | 18 | 225 | 198 | 193 | 178 |
| | 60 | 21 | 300 | 270 | 261 | 240 |
| | 80 | 25 | 355 | 317 | 310 | 285 |
| | 100 | 28 | 419 | 385 | 380 | 364 |
| 1800 | 30 | 30 | 254 | 236 | 234 | 216 |
| | 60 | 35 | 340 | 317 | 314 | 291 |
| | 80 | 38 | 400 | 370 | 370 | 344 |
| | 100 | 42 | 433 | 400 | 400 | 372 |
| 2200 | 30 | 34 | 276 | 257 | 255 | 238 |
| | 60 | 38 | 360 | 340 | 340 | 315 |
| | 80 | 43 | 415 | 388 | 388 | 365 |
| | 100 | 50 | 423 | 392 | 392 | 371 |
| 3000 | 30 | 69 | 305 | 300 | 297 | 287 |
| | 60 | 74 | 373 | 364 | 364 | 342 |
| | 80 | 79 | 395 | 384 | 384 | 377 |
| | 100 | 83 | 427 | 415 | 415 | 407 |

to be useable for the next experiment. Unfortunately, the weighing process is not practical with the full-sized filter on account of the large experimental error caused by the order-of-magnitude difference between filter mass (1 kg and more) and collected soot mass (10–30 g). Thus, in the case of full filters there is no such possibility of cross-checking the soot mass.

## 4 COMPUTATIONAL ASSISTANCE OF EXPERIMENTS

As explained above, the aim of the single-channel filter experiments is the estimation of the product $(\rho k)_p$ of soot collected in the filter channel. A calculation method, illustrated in this section, was employed in the processing of experimental results. An accurate knowledge of the mass collected in the filter channel is necessary accurately to estimate the product $(\rho k)_p$. To this end, the single-channel filter was weighed before and after each loading experiment, and the soot mass determined in this way was employed as an input factor in the computer calculation written to support the pressure drop characteristic calculations. The output of this calculation, which is written in Fortran 77, is a graph of vessel pressure as a function of time during the discharge process. The calculation can be done either for a single channel (made of cordierite or SiC), clean or loaded with soot, or just for the discharge nozzle, without any filter channel connected, for validation purposes.

Two factors are unknown and must be tuned in this calculation process:

(a) the discharge coefficient $C_D$,
(b) the above-mentioned $(\rho k)_p$ product.

These two factors govern the pressure drop characteristics of the experimental apparatus. The tuning process is based on the comparison of the experimentally measured and the calculated discharge characteristic of vessel pressure versus time.

The discharge coefficient of the nozzle is tuned on the basis of the discharge through new single-channel filter specimens made of cordierite and SiC (Figs 10a and b). Afterwards, the single-filter specimens are loaded and connected to the real engine exhaust line as previously described. Subsequently, they can be connected to the measuring device and the experimental curve of the discharge process can be recorded. The next step is to weigh the filter specimen, thus measuring the soot mass collected in the minifilter. The tuning process for the estimation of $(\rho k)_p$ is based on fitting the experimental discharge curve of the loaded minifilter to the calculated curve with the computer calculation process. The main input factors to the computer calculation are the initial vessel pressure, the vessel air temperature, the discharge coefficient, the dimensions of the single channel, the substrate thickness, $E_s$, and permeability, $k_s$, the soot mass in the channel and the $(\rho k)_p$ product (this last is tuneable as already explained).

### 4.1 Physics of the process employed in the computation

During discharging of the vessel air, air passes through a nozzle (or throat) that concurs with the inlet of the channel. Therefore, it is possible to have choked conditions of flow, or sonic velocity ($Ma = 1$), in the throat. For this reason, the computer calculation checks where there are choked or subcritical flow conditions and makes use of the corresponding formulae at each calculation time step. In choked flow, the following formula is employed:

$$\dot{m}_{\text{real}} = \frac{C_D A_T p_0}{\sqrt{RT_0}} \gamma^{1/2} \left\{ \frac{2}{\gamma + 1} \right\}^{(\gamma+1)/2(\gamma-1)} \tag{4}$$

On the other hand, in the subcritical flow condition, the

following formula is employed:

$$\dot{m}_{\text{real}} = \frac{C_{\text{D}} A_{\text{T}} p_0}{\sqrt{RT_0}} \left(\frac{p_{\text{T}}}{p_0}\right)^{1/\gamma} \left\{\frac{2\gamma}{\gamma - 1}\left[1 - \left(\frac{p_{\text{T}}}{p_0}\right)^{(\gamma-1)/\gamma}\right]\right\}^{1/2} \tag{5}$$

The computer calculation continuously checks the pressure ratio and compares it with the critical pressure ratio $p_{\text{T}}/p_0$, which is taken to be equal to 0.528 (air at near-ambient pressure and temperature conditions can be assumed to behave like an ideal diatomic gas, $\gamma = 1.4$). The discharge coefficient $C_{\text{D}}$ is a flow coefficient that is mainly a function of the shape of the passage and needs always to be experimentally determined.

The vessel pressure at any time step is given by the equation of state

$$p_0 V = m_{\text{v}} R T_0 \tag{6}$$

where $p_0$ and $T_0$ are the pressure and temperature inside the vessel or, in other words, the stagnation pressure and temperature. For the throat region, the following expression is valid:

$$\dot{m}_{\text{real}} = \rho_{\text{T}} u_{\text{T}} A_{\text{T}} \tag{7}$$

The filtration velocity, $U$, is correlated with the throat velocity or the real mass flow, $\dot{m}_{\text{real}}$, by means of the continuity equation

$$\rho_{\text{T}} u_{\text{T}} A_{\text{T}} = \rho_{\text{ch}} U A_{\text{ch}} \tag{8}$$

and so

$$\dot{m}_{\text{real}} = \rho_{\text{ch}} U (4Lw) \tag{9}$$

or

$$U = \frac{\dot{m}_{\text{real}}}{\rho_{\text{ch}} (4Lw)} \tag{10}$$

### 4.2 Computer calculation procedure

The computer calculation procedure consists of two discrete parts, as can be seen from the flow chart in Fig. 9. In the first part, the real air mass outflow from the vessel is calculated by equation (4) for choked flow or by equation (5) for subcritical flow. In the second part, the vessel pressure is calculated using the state equation (6). During the discharging process, two conditions of flow may prevail: choked or subcritical flow. The mass flowrate at each time step is computed according to the critical pressure ratio using the appropriate formula. The mass flowrate at each time step is computed according to the critical pressure ratio using the appropriate formula. From the second time step onwards, the vessel pressure is iteratively determined from the outgone mass for the $i$th time step ($\dot{m}_{\text{real}}$ has already been calculated)

$$\mathrm{d}m_i = \dot{m}_{\text{real}i}\, \mathrm{d}t \tag{11}$$

and the remaining mass in the vessel

$$m_{\text{v}(i)} = m_{\text{v}(i-1)} - \mathrm{d}m_{(i-1)} \tag{12}$$

which updates the vessel pressure by means of equation of state (6).

Then, the filtration (superficial) velocity, $U$, is calculated by equation (10). The latter velocity is used in $(\Delta p)_{\text{c}}$ calculation with the aid of equation (3). Also, because the filter is discharging to the free atmosphere, $\Delta p$ can be assumed equal to the difference between the pressure at the throat and atmospheric pressure:

$$\Delta p = p_{\text{T}} - p_{\text{atm}} \tag{13}$$

and from equation (13)

$$p_{\text{Tc}} = (\Delta p)_{\text{c}} + p_{\text{atm}} \tag{14}$$

Thus, two pressure values have been estimated for the throat region. This is a checkpoint for the code. The above values must satisfy the condition of equality in the same region (throat). If the difference between the two calculated pressures is small enough, or $(p_{\text{TG}} - p_{\text{Tc}})/p_{\text{TG}} < 0.001$, then the calculations are continued for the next time step. Otherwise, the previously mentioned process is repeated with another guessed pressure value in the throat until the solution for this time step has converged. Afterwards, the computation code enters the next time step calculations and this procedure terminates when the vessel pressure has reached ambient pressure.

## 5 RESULTS AND DISCUSSION

### 5.1 Single-channel traps

As already mentioned, the final objective of the combined experimental and computational method is the determination of values for the product $(\rho k)_{\text{p}}$. However, a validation of the computer calculation procedure is necessary. Thus, a set of validation tests was first performed. The validation procedure involved the determination of the discharge coefficient, $C_{\text{D}}$, for both single-channel filter specimens (made from cordierite and SiC respectively). These two single-channel filters are taken from full-scale filters, as explained above, and their main features are presented in Table 1. Each validation test consisted of a particular experiment, in which each minifilter was connected to the vessel and the compressed air was discharged through the filter channel. The validation curves are presented in Fig. 10. It can be seen that the computer code behaves better with the SiC minifilter, whereas in the cordierite case there is a small but observable deviation from the experimentally measured curve.

As a next step, loading experiments were performed with soot emitted by the engine operating on 25 ppm DPX9-doped fuel at the previously described operation points (see Table 4). After the loading procedure, the minifilter was weighed and subsequently connected to

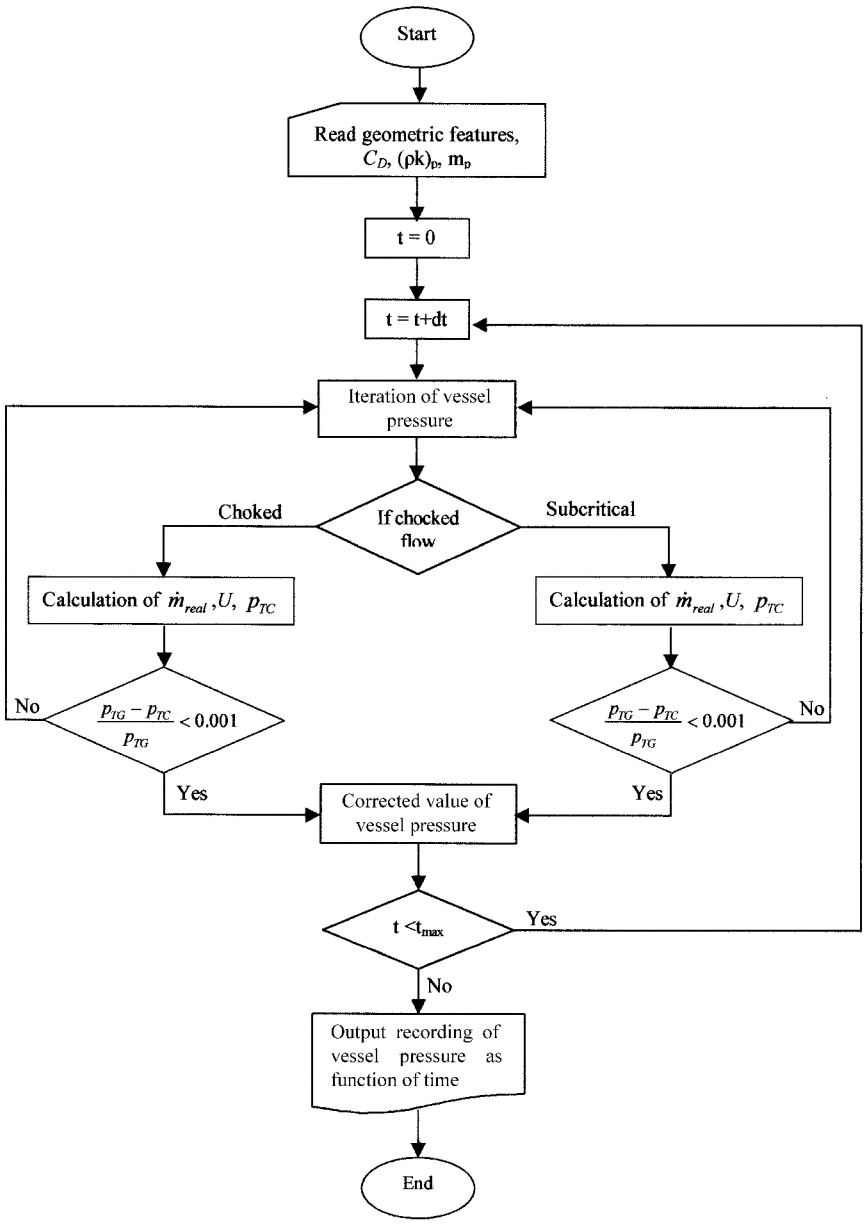


**Fig. 9** Computer calculation flow chart

the measuring device, where the pressure–time curve was obtained.

Two representative curves of vessel pressure–time characteristics with a loaded cordierite minifilter that were employed in the tuning process are presented in Fig. 11a. The tuning is implemented by comparison between the experimental and computational curve. The computation is seen to behave well with the simulation of the two experiments, resulting in different $(\rho k)_p$ product values for the two different soot loading levels. For the cordierite case it is observed that the greater soot mass retards the discharge process of the pressurized air, and $(\rho k)_p$ decreases as the mass of the accumulated soot increases. The results for a number of tuned values of $(\rho k)_p$ as a function of engine operation point are presented in Table 5 and Fig. 12a. According to these results, the variation in $(\rho k)_p$ with the engine operation point over the low and medium rnge of speed and load is measured in the range from $3.5 \times 10^{-12}$ to $1.15 \times 10^{-11}$ kg/m.

In order to investigate the same effect with a different filter material, a new set of measurements was performed with the SiC single-channel filter. Two more coupled curves of experimental and calculated pressure discharge curves are presented in Fig. 11b. Also, in this case it is observed that for higher soot mass the air discharges slower and the $(\rho k)_p$ value decreases, and the values determined lie in the same range as with the cordierite

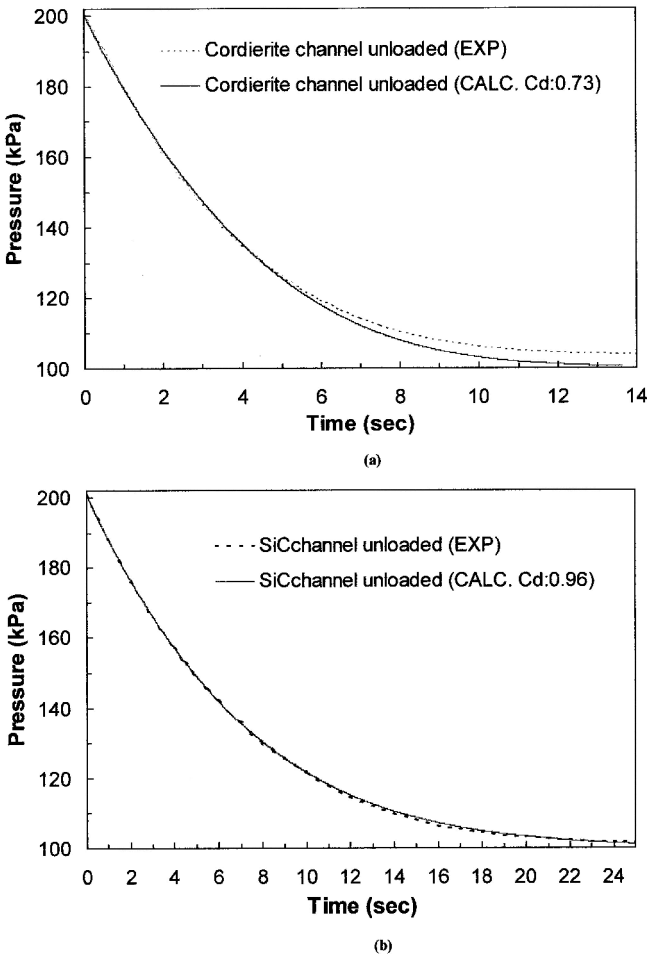


**Fig. 10** Code validation $C_D$ estimation curves for (a) cordierite and (b) SiC single-channel filters

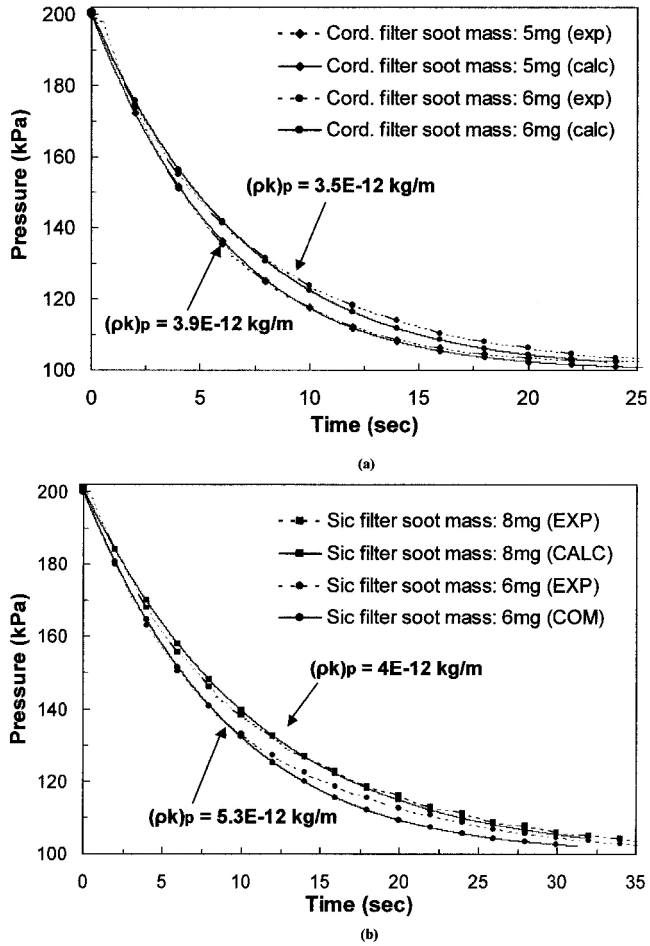


**Fig. 11** Representative curves of parameter $(\rho k)_P$ tuning at various filter loads and engine operation points: (a) cordierite single-channel filter; (b) SiC single-channel filter

samples, as would be expected. The values of the determined $(\rho k)_P$ product as a function of engine operation point are presented in Fig. 12b. The results for the two types of filter material are summarized and presented in Table 5. Here it should be mentioned that similar research carried out with an IDI engine by Sorenson *et al.* [**15**] resulted in lower $(\rho k)_P$ values. This could be attributed to the significantly higher VOF content of the exhaust gas of indirect injection diesel engines.

A more detailed analysis of the above-mentioned experimental results shows that the $(\rho k)_P$ product not only depends on the accumulated soot mass but also is a function of engine operation point. That is, the pressure discharge–time curve employed in the indirect determination of the soot loading of each filter channel is affected at least by the collected soot mass, the engine speed and torque and the presence of a fuel additive component. Furthermore, the role of adsorbed hydrocarbons on the soot particulate and the ceramic substrate must be considered [**16**], and research in this subject is under way in LTTE/UTh.

As a general conclusion, for both types of filter material it can be observed that the higher soot mass is associated with a decrease in the $(\rho k)_P$ parameter value. This is apparent in Fig. 13, in which the $(\rho k)_P$ parameter is determined for various filter loading experiments at the same engine operation point. This could mean that the decrease in soot permeability prevails over the increase in soot density during the assumed compression of the particle layer at higher soot loading levels.

### 5.2 Full-scale filters

As reported above, experiments with full-scale filters were also performed in order to investigate the exhaust flow characteristics and soot mass distribution along the filter channels during the loading and regeneration procedure. Figure 14 presents the vessel pressure discharge curves obtained at selected channels equidistantly positioned along a filter diameter, after loading at the following two characteristics points:

**Table 5** Summarized results for $(\rho k)_p$ parameter for various single-channel filter loads and engine operation points

| Operation point | | Cordierite single-channel filter | | SiC single-channel filter | |
|---|---|---|---|---|---|
| Speed (r/min) | Torque (N m) | Soot mass collected (mg) | $(\rho k)_p$ (kg/m) | Soot mass collected (mg) | $(\rho k)_p$ (kg/m) |
| 1250 | 30 | 10 | $7.00 \times 10^{-12}$ | 4 | $5.50 \times 10^{-12}$ |
| 1250 | 60 | 12 | $1.00 \times 10^{-11}$ | 8 | $5.60 \times 10^{-12}$ |
| 1250 | 80 | 5 | $3.90 \times 10^{-12}$ | 6 | $5.30 \times 10^{-12}$ |
| 1250 | 100 | 7 | $6.40 \times 10^{-12}$ | 7 | $6.20 \times 10^{-12}$ |
| 1800 | 30 | 9 | $7.95 \times 10^{-12}$ | 8 | $1.10 \times 10^{-11}$ |
| 1800 | 60 | 5 | $4.10 \times 10^{-12}$ | 8 | $5.85 \times 10^{-12}$ |
| 1800 | 80 | 4 | $4.10 \times 10^{-12}$ | 6 | $3.80 \times 10^{-12}$ |
| 1800 | 100 | 4 | $4.80 \times 10^{-12}$ | 6 | $3.70 \times 10^{-12}$ |
| 2200 | 30 | 10 | $6.00 \times 10^{-12}$ | 8 | $4.00 \times 10^{-12}$ |
| 2200 | 60 | 9 | $7.60 \times 10^{-12}$ | 7 | $3.50 \times 10^{-12}$ |
| 2200 | 80 | 12 | $1.15 \times 10^{-11}$ | 8 | $8.30 \times 10^{-12}$ |
| 2200 | 100 | 3 | $3.90 \times 10^{-12}$ | 4 | $3.40 \times 10^{-12}$ |
| 3000 | 30 | 5 | $4.70 \times 10^{-12}$ | 7 | $3.50 \times 10^{-12}$ |
| 3000 | 60 | 6 | $3.50 \times 10^{-12}$ | 5 | $5.00 \times 10^{-12}$ |
| 3000 | 80 | 7 | $1.00 \times 10^{-11}$ | 6 | $9.10 \times 10^{-12}$ |
| 3000 | 100 | 8 | $1.10 \times 10^{-11}$ | 5 | $9.90 \times 10^{-12}$ |

| Speed (r/min) | Load (N m) | Final back pressure (mbar) | Wall temperature, centre (°C) | Wall temperature, periphery (°C) |
|---|---|---|---|---|
| 2000 | 90 | 150 | 390 | 370 |
| 2000 | 90 | 450 | 410 | 390 |

The coincidence of the curves in the case of filter loading to 150 mbar back pressure indicates a uniform distribution of soot mass (and possibly exhaust gas flow). This is not observed in the case of 450 mbar filter back pressure. As can be seen, at least two different zones are observed as the measuring device is removed from the central (hotter during operation) to the outer (colder during operation) channels, since the pressurized air is shown to discharge faster through the central channels than through the circumferential channels. This could be attributed to the effect of VOF present in the thick particulate layer, which should preferentially condense on the colder outer channels after engine stop, thus differentiating permeability characteristics between filter core and periphery channels, which would be expected to be comparable during hot operation.

The role of the wall temperature gradient during an incomplete regeneration in the soot mass distribution is further investigated with the experimental results of Fig. 15. The resultant curves refer to the determination of the product $(\rho k)_p$ in central and peripheral channels after filter regeneration at an engine speed of 2800 r/min and a load of 180 N m, which results in the filter wall temperature varying from 610 °C (filter centre) to 580 °C (filter periphery). In order to exclude any secondary effects from fuel additive residuals, the filter was loaded without a fuel additive at a speed of 2000 r/min and a load of 90 N m up to a back pressure of 150 mbar. The variation in the vessel discharge curves moving from the centre to the periphery indicates incomplete regeneration at the filter periphery. This is due to the lower wall temperature measured (thermal regeneration!). This behaviour during a partial regeneration would result, during a subsequent loading phase, to a significant differentiation of the exhaust flow distribution, with the exhaust flowing mainly through the central region of the filter. This mechanism could also explain the different loading behaviour between a new and a previously incompletely regenerated filter.

Finally, the role of fuel additive was also investigated. After prolonged filter operation with the engine having consumed about 1000 l of diesel fuel doped with 25 ppm Ce additive running in loading and regeneration modes at various operation points, a new set of measurements along a filter diameter was performed. In this case the filter was completely regenerated. The results of Fig. 16 indicate that the pressurized air discharges faster through the circumferential channels than through the central channels. This means that the fuel additive ash is concentrated mainly on the central region of the filter. Again, such an observation can be explained by the previously proposed mechanism, because the central filter region tends to regenerate more completely than the outer region, thus attracting a higher total exhaust flow over a long period of time.

## 6 CONCLUSIONS

1. A measuring device and a computer calculation procedure have been developed in order to assist the experimental study of soot loading distribution in wall-flow diesel particulate filters.
2. The measuring device records vessel pressure versus time as the pressurized air from a vessel discharges through selected channels of a particulate trap or

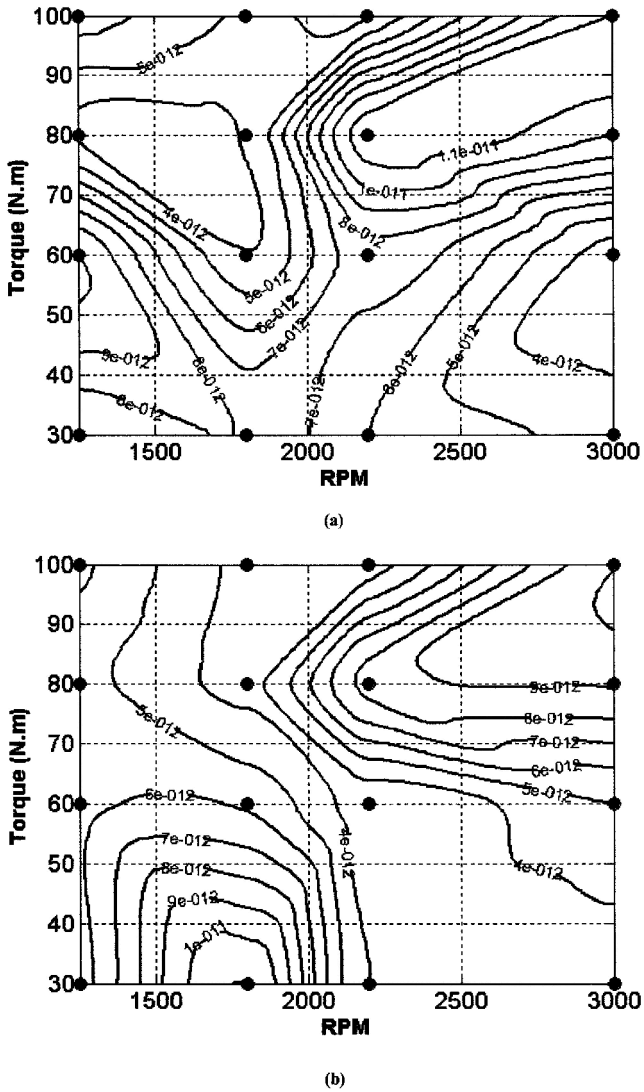


**Fig. 12** Map of parameter $(\rho k)_P$ as a function of the engine operation point: (a) cordierite single-channel filter; (b) SiC single-channel filter

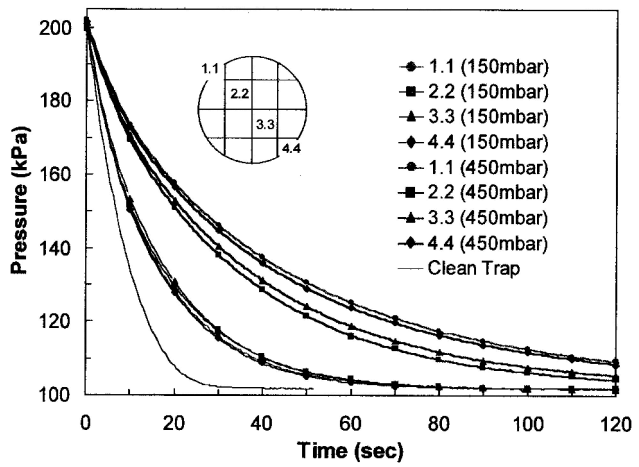


**Fig. 14** Pressure drop measurements along a diameter for a full-sized filter loaded up to 150 mbar and up to a 450 mbar pressure drop (measured at 2000 r/min and 90 N m)

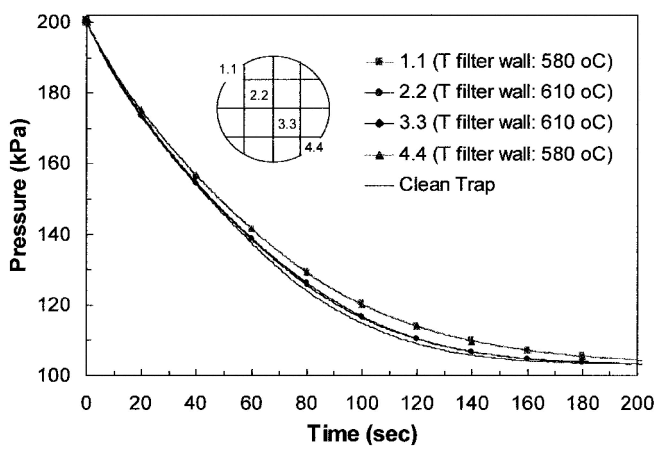


**Fig. 15** Pressure drop measurements along a diameter after the regeneration of a filter loaded up to 150 mbar at 2000 r/min and 90 N m with 0 ppm fuel additive

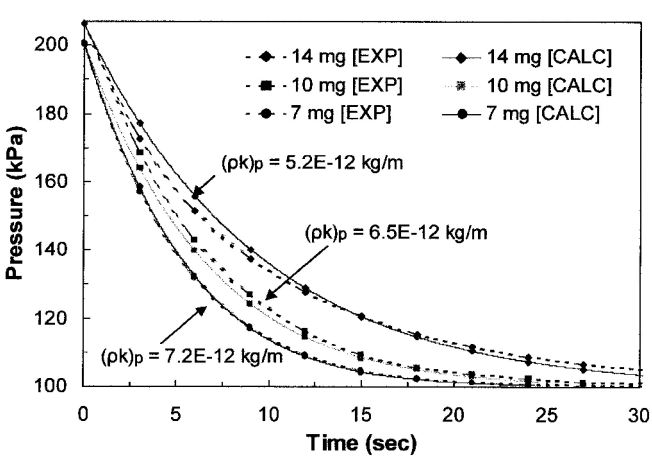


**Fig. 13** Calculation of $(\rho k)_P$ values for various loading levels with the engine running at the same operation point (3000 r/min, 40 N m)

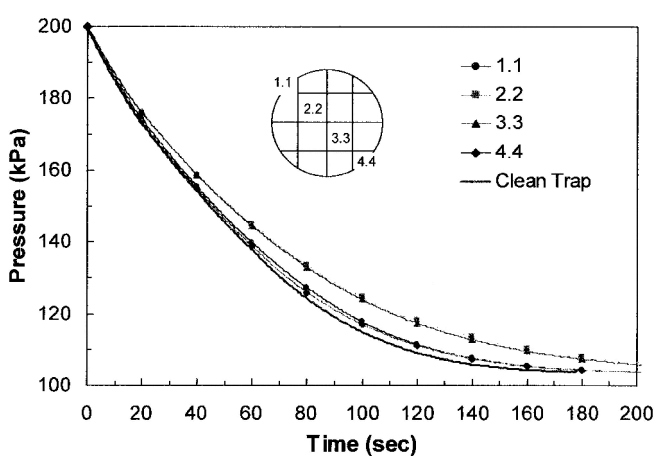


**Fig. 16** Pressure drop measurements for a complete regenerated filter after the engine has consumed about 1000 l of diesel fuel doped with 25 ppm additive (ash effect)

through single-channel specimens of cordierite and SiC.

3. The pressure recordings taken by this simple and easily implemented device and methodology are employed in the estimation of the product $(\rho k)_p$, as demonstrated in this paper.
4. The results indicate that the product $(\rho k)_p$ (soot layer density times permeability) for the specific engine and filter combination lies in the range from $3.5 \times 10^{-12}$ to $1.15 \times 10^{-11}$ kg/m, both for a cordierite and an SiC filter fitted to the specific engine.
5. Study of the soot layer density times permeability variation indicates a significant influence of the engine operating point and also soot loading.
6. The above simple $(\rho k)_p$ estimation methodology may be extended to give an indicative picture of the distribution of soot and fuel additive ash loading among the channels of a full-sized filter, as shown in selected cases in this paper.
7. Further development of the above methodology is expected to improve confidence in the accuracy of estimation of soot and additive ash loading in full-sized filters.

## REFERENCES


1 **Walsh, M. P.** Global trends in diesel emissions regulations—a 2001 update. SAE paper 01-0183, 2001.

2 **Clerc, J. C.** Catalytic diesel exhaust aftertreatment. *Appl. Catalysis B: Environ.*, 1996, **10**, 99–115.

3 **Johnson, J. H., Bagley, S. T., Graz, L. D.** and **Leddy, D. G.** A review of diesel particulate control technology and emissions effects. SAE paper 940233, 1994.

4 **Farrauto, R. J.** and **Voss, K. E.** Monolithic diesel oxidation catalysts. *Appl. Catalyis B: Environ.*, 1996, **10**, 29–51.

5 **Neeft, J. P. A., Makkee, M.** and **Moulijn, J. A.** Catalysts for the oxidation of soot from diesel exhaust gases. I. An exploratory study. *Appl. Catalysis B; Environ.*, 1996, **8**, 57–78.

6 **Neeft, J. P. A., Schiper, W., Makkee, M.** and **Moulijn, J. A.** Feasibility study towards a Cu/K/Mo/(Cl) soot oxidation catalyst for application in diesel exhaust gases. *Appl. Catalysis B: Environ.*, 1997, **11**, 365–382.

7 **Johnson, T. V.** Diesel emission control in review. SAE paper 01-0184, 2000.

8 **Salvat, O., Marez, P.** and **Belot, G.** Passenger car serial application of a particulate filter system on a common rail direct injection diesel engine. SAE paper 01-0473, 2000.

9 **Koltsakis, G. C.** and **Stamatelos, A. M.** Catalytic automotive exhaust aftertreatment. *Prog. Energy Combust. Sci.*, 1997, **23**, 1–39.

10 **Bissett, E.** and **Shadman, F.** Thermal regeneration of diesel-particulate monolithic filters. *AIChE J.*, May 1985, **31**(5), 753.

11 **Koltsakis, G. C.** and **Stamatelos, A. M.** Modeling catalytic regeneration of diesel particulate traps. *Industrial and Engng Chem. Res.*, 1996, **35**, 2–13.

12 **Koltsakis, G. C.** and **Stamatelos, A. M.** Modes of catalytic regeneration in diesel particulate filters. *Industrial Engng Chem. Res.*, 1997, **36**, 4155–4165.

13 **Pontikakis, G., Stamatelos, A., Bakasis, K.** and **Aravas, N.** 3-D catalytic regeneration and stress modeling of diesel particulate filters by ABAQUS FEM software. SAE paper 01-1017, 2002.

14 **Versaevel, P., Colas, H., Rigaudeau, C., Noirot, R., Koltsakis, G. G.** and **Stamatelos, A. M.** Some empirical observations on diesel particulate filter modeling and comparison between simulations and experiments. SAE paper 01-477, 2000.

15 **Sorenson, S. C., Hoj, J. W.** and **Stobbe, P.** Flow characteristics of SiC diesel particulate filter materials. SAE paper 940236, 1994.

16 **Stratakis, G. A.** and **Stamatelos, A. M.** Thermogravimetric analysis of soot emitted by a modern engine run on catalyst-doped fuel. Submitted to *Particulate Sci. and Technol.*, 2002.